Magnetic properties map of a CoFe and NiFe multi-layer compound with a Ruthenium spacer wedge

Juan Felipe Builes

Industrial Engineer

U.S. Department of Energy Office of Science, Science Undergraduate Laboratory Internship (SULI)

Lawrence Berkeley National Laboratory, Berkeley, California

Arts et Métier ParisTech, Metz, France

June 24, 2015

Prepared in partial fulfillment of the requirements of the U.S. Department of Energy Office of Science, Science Undergraduate Laboratory Internship (SULI) under the direction of Alpha T. N'Diaye in the Advanced Light Source Division at Lawrence Berkeley National Laboratory.

Juan Felipe Builes
SULI Spring 2015

ABSTRACT

This project is centered on magnetic mapping with soft x-rays, it had two components: an experimental part and a technical part. The experimental part was measuring x-ray absorption spectroscopy, x-ray magnetic circular dichroism, and magnetic hysteresis loop at the Beamline 6.3.1 on a sample of two magnetic layers, separated by a 3.1nm thin Ruthenium wedge. Using x-rays, one investigated how the magnetic interaction between the two significantly depends on the thickness of the Ruthenium separator. It was observed a high influence of the magnetic properties of the layers and the Ruthenium spacer thickness.

The technical part consisted in developing a Graphical User Interface (GUI) application in Python to generate the input files for automated experiments at the Beamline. Conventionally, only a few absorption spectra were measured at a time. With the new application, it is user friendly to run hundreds of scans in a row, allowing the users to make better use of the Beamline's capabilities.

Key Words: x-ray, magnetism, circular dichroism, hysteresis-loop, spectroscopy, Graphical User Interface.

1. INTRODUCTION

Magnetism is a physical phenomenon that plays a big role in current and future technologies. Therefore, the control of magnetic material parameters, such as a high magnetic moment for strong magnets or some specific behaviors of the "magnetization memory" or hysteresis such as a low coercive field and constant susceptibility needed for new materials in DC transformers, or a high coercive field particularly for ferromagnets as used in motors and generators, are very desired by the industry.

The strongest permanent magnets produced are based on rare earth elements. The biggest rare earths deposits in 2014 were found in China (39.3%), Brazil (15.7%), United States (9.3%), and other countries (29.3%) [3]. These materials are limited and non-renewable. Although, our industry depends on such magnets and only a few key players dominate the market.

The idea was to analyze the influence of the thickness of a Ruthenium wedge that separates two magnetic bilayers and the biquadratic interlayer coupling of the CoFe and NiFe, which is the antiparallel orientation between the magnetic domains of the layers CoFe and NiFe. These characteristics are used for spintronics and hard drive reading heads. One experimentally analyzed if the magnetic bi-layers follow the Stoner-Wohlfarth model [1], which states that the sample can be interpreted as a single domain ferromagnetic material. It is used to model small magnetic particles in magnetic storage, biomagnetism, rock magnetism, and paleomagnetism.

It was created an application in Python with a friendly Graphical User Interface (GUI) that helps the users to easily create a script that runs the spectroscopy in the Beamline

6.3.1 for their experiments. Before, the Beamline users could create the scan files with only one group of parameters. Now, the application allows them to insert several groups of parameters in a single scan file and gather hundreds of spectra in a row with the help of one interface. Such scans were only done by ALS scientists before and had not been available to general users. The application processes spectroscopy data maps of a few hundred scans with a few hundred data points each.

2. METHODS

2.1. Sample preparation

The sample is a multi-layer compound of Ru 5nm, MnIr 15nm, $Co_{70}Fe_{30}$ 10nm, Ru wedge 0-3.1nm, $Ni_{81}Fe_{19}$ 10nm, Ru 4nm and MgO. It was prepared by magnetron sputtering in the group of Jan Schmalhorst, University of Bielefeld, Germany. See Fig 1.

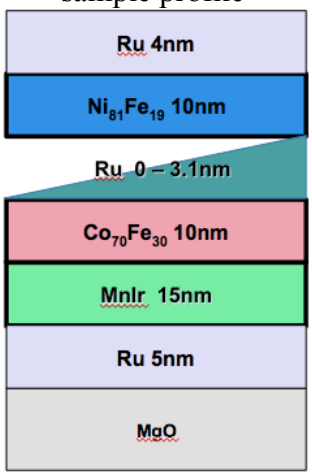

FIG. 1: Multi-layer sample profile

For the measurements, the sample was divided in seven sections where one could analyze the influence of the Ruthenium wedge. The samples were mounted ex-situ and transferred into an ultra-high vacuum chamber with a base pressure of 10^{-8} Torr and assuring a pressure lower than 10^{-6} Torr for measurements. The data was gathered at room temperature.

The research at Beamline 6.3.1 at the Advanced Light Source (ALS) in Lawrence Berkeley National Laboratory [4] employs a mapping approach using soft x-ray spectroscopy techniques. This mapping consisted in analyzing and comparing: firstly the XAS, secondly the XMCD, and thirdly the Magnetic Hysteresis (MH) loop for many spots on one sample with locally varying properties.

Alternatively, one can measure the material x-ray absorption intensity by two complementary techniques: the total electron yield (TEY) and the luminescence. The TEY by quantifying the total flux of electrons ejected from one suborbital at a certain photon energy (or wavelength of the beam) and recording the electric current between

sample and ground, and the luminescence by measuring the photons created by the MgO substrate at the bottom of the sample. The Fig 2 explains both techniques.

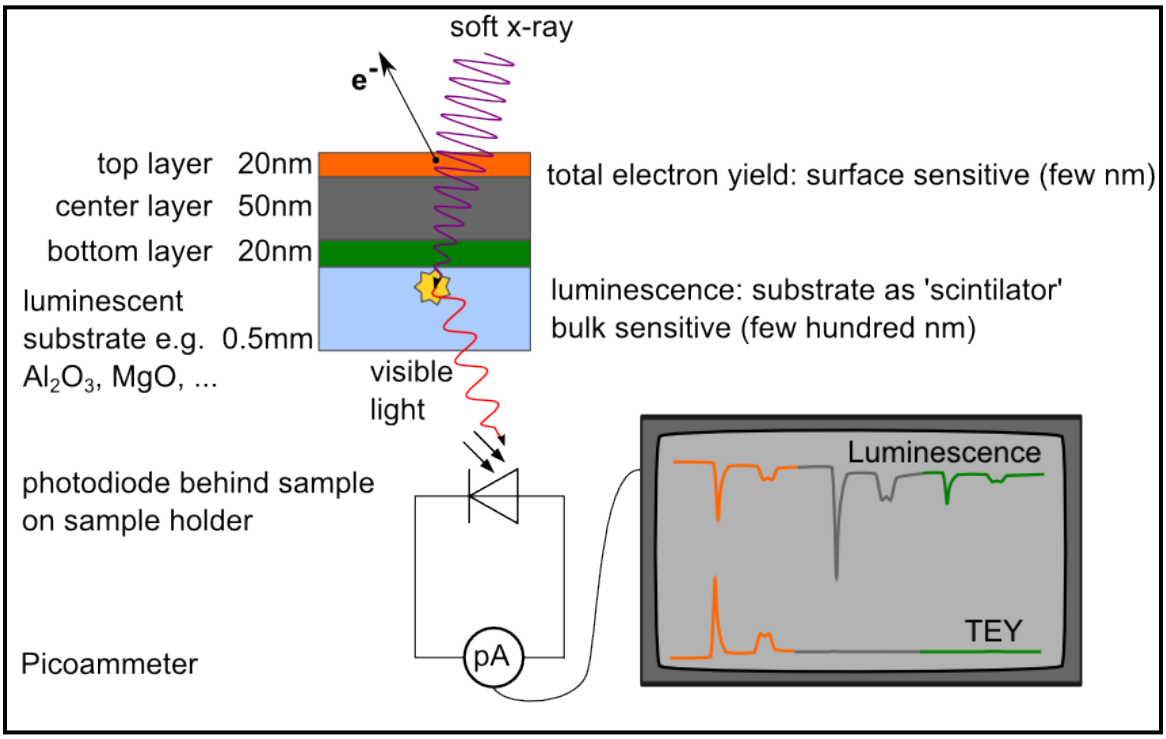

FIG. 2: TEY and luminescence representation.

2.2. XAS measurements

In X-ray absorption spectroscopy the sample was exposed to soft x-rays and while the energy of the light was tuned to the absorption edges, one measured the absorption of x-rays by measuring the intensity of x-rays that was transmitted through the sample. This was only possible for the top layers. The XAS was measured to the L-edges of the Mn, Fe, Co, and Ni. [5]

2.3. XMCD measurements

The X-ray magnetic circular dichroism refers to the changes of the absorption of circular polarized light when switching the direction of polarization with respect to the sample magnetization [6]. The XMCD was measured in a photon energy range from 630eV to 880eV, according to the L-edges energy requirement of each element. It was obtained by measuring the TEY at the L-3 and L-2 edges of the Mn, Fe, Co, and Ni. The magnetic field applied was $\pm$0.5 T.

2.4. MH measurements

The magnetic hysteresis loop represents the relation between an increasing/decreasing external magnetic field *H* and the magnetization *M* in magnetic materials, hence it is also called MH loop. The MH was not only measured in order to extract the remanence and coercivity but mainly to gain information about the interaction of the two layers. The element specificity of the XMCD allows measuring the MH loop of Nickel, which is only present in the upper magnetic layer; and also Cobalt, which is only present on the lower magnetic layer separately. The magnetic field applied was swept from 34 mT to -34 mT in steps of 0.08 mT.

2.5. Script manager application

The application was written in Python 2.7.8 [7] and the Integrator Developer Environment (IDE) was PyCharm CE 4.0.4 [8]. The external libraries used were Tkinter, Scipy, Numpy, Math, ConfigParser, and os.path. They were downloaded by Anaconda package [9]

The format of the scan file is in .txt format, which is read by the Beamline software. This file must have some characteristics, the motor names have to be written as headers separated by a tab and all the data contained have to be arranged in columns separated by a tab. The configuration file is .ini format. It contains all the essential variables and values in order to load a certain configuration in the GUI. It is written under the .ini format convention.

For the documentation, all the code is commented and separated respectively in classes and functions in order to be modified or adapted to the user need. As Fig 11 shows.

3. RESULTS AND DISCUSSION

3.1. Experimental component:

Observing the Fig 4, the TEY of the Fe and Ni present a constant and strong absorption intensity for L-edges. In the other hand, Co does not have a constant signal in TEY being 15nm under the surface, and it becomes lower as the Ru-Wedge grows, decreasing from (a) 0.24 to (c) 0.12. By contrast, the luminescence signal displays a constant absorption for all layers independent to the Ru-Wedge thickness. The XAS graphs in Fig 1 were normalized to 1.

The TEY on Fig 4(a)(c) show that the Mn L-edges peaks are split. Comparing the previous graphs with the Mn oxides samples spectra in Fig 5 [6], it shows that Mn is at least partially oxidized. Although the sample is grown on MgO substrate, it can be discarded that the unexpected split peaks at the TEY of the Mn L-edges are Mg K-binding at 1303eV, considering that one can observe some peaks in the luminescence

from Fig 4(b)(d) between 652eV and 690eV, which corresponds to the light of 1305eV to 1380eV from the second order diffraction of the monochromator of the beamline.
Observing that the Mn X-ray absorption is independent to the Ru-Wedge thickness one can also infer that there is unexpected Mn above the Ru-Wedge layer.

Comparing the Fig 6 (a) with (b), the XMCD by (a) TEY presents less noise than the (b) luminescence finding less peaks and a smoother function. The XAS and XMCD results follow the expected behavior for Fe, Co and Ni demonstrating consistency in the sample.

Observing the Fig 7, the (b) luminescence MH is noisier than by (a) TEY, presenting an average standard deviation of 0.022 for the TEY and 0.141 for the luminescence. All the MH scans present the same noisy quality pattern. The data was obtained for the Fe MH loops at 707.1eV beyond the saturation points at $\pm$4mT. All graphs were normalized to 1.

The biquadratic coupling exchange is observed in the CoFe and NiFe layers on the Fig 8 (a) and (e). In (a) when the magnetic field goes from +34mT to -34mT, while there is still a positive magnetic field applied to the sample, the NiFe domains switch to an antiparallel alignment at +11mT; also when the magnetic field goes from -34mT to +34mT, under a negative magnetic field applied, the NiFe domains switch to an antiparallel alignment at -15mT. A similar biquadratic coupling exchange is observed in graph (e) for the NiFe layer at +3mT decreasing the magnetic field from positive to negative.

Comparing the experimental MH loops with the SW simulation in different Ruthenium thicknesses (d_{ru}), in Fig 8 (a) and (b) is observed an equal behavior of the loops and the

magnetic saturation (Hs) is presented at the same magnetic field in both layers. The Figure 8 (c) and (d) present a perfect overlap in the Hs in both layers. In Figure 8 (e) and (f) it is seen that the magnetization of the loops have the similar behavior, part of Ni loops is outside Co loop, but it is presented in different directions. This is explained because the MnIr is an antiferromagnet with a fixed magnetic domain orientation due to the sample preparation. The Ru layer is so thick that the FeNi and FeCo are independent from each other and the exchange bias to the MnIr layer dominates the behavior of FeCo. Fig 8 (b)(d)(f) were obtained by the group of Jan Schmalhorst, our collaborators of the University of Bielefeld in Germany by the numerically simulated hysteresis loops based on the Stoner-Wolfarth single domain model.

The Fig 9 represents the Co MH evolution by luminescence within a Ruthenium thickness from 0.34nm to 3.10nm. It is identified a high remanence and a low coercivity. One can observe a magnetic saturation at 5mT and -7mT when $d_{ru} = 0.34$nm; in the other hand, when $d_{ru} > 2.48$nm the magnetic saturation is -2mT and -2.7mT, almost instantly.

The Fig 10 represents the Ni MH evolution by luminescence within a Ruthenium thickness from 0.31nm to 3.10nm. When the $d_{ru} > 2.35$nm a high remanence and a low coercivity are identified. However, when d_{ru} is greater than 2.01nm and lower than 2.35nm a low remanence and a high coercivity are observed, accompanied by a biquadratic coupling exchange between the external magnetic field and the NiFe layer. NiFe magnetic saturation is much higher than the CoFe saturation, presented at 157mT and -16mT when $d_{ru} = 2.10$nm; however, when $d_{ru} > 2.48$nm the magnetic saturation is -1mT and -3mT, even faster than the CoFe layer.

In Fig 10, the red background represents the MH of the CoFe layer, delimited by its magnetic saturation, which is insignificant compared to the NiFe saturation at $d_{ru} < 2.35nm$. Nevertheless, when $d_{ru} > 2.35nm$ it is presented an alignment of the MH loops, with a similar remanence, coercivity, and magnetic saturation.

3.2. Technical component:

The script manager graphical application allows the user to create a scan file for the Beamline for several motors simultaneously. A scan file is arranged by a motor, an input type and some values. A motor is the main parameter that conducts the Beamline, it can be the position of the sample holder (x, y, z coordinates), the angle of incidence of the x-ray with the sample, or the external magnetic field applied to the sample. The input type determines the way the algorithm processes the values inputted in the 'values box', they can be sorted as a range from a lower limit to a upper limit by a desired step, as a list of numbers, or as a flying configuration that will create a fast scan. The list of values define the points and sample conditions at which data form the beamline is to be acquired. The list is saved as a scan file.

Fig 3 shows the GUI of the application. The interface is divided in three segments:

1. The top, where the user selects the motor and the input type, inputs the values and add rows or input type according to the desired scan.
2. The bottom right, where one can visualize the information of the scan configuration, estimate the time of the experiment, and leave any commentaries for the configured file.

3. The bottom left, where the user can execute different actions, whether reset the GUI, load or save a configuration, write a scan file or close the software application.

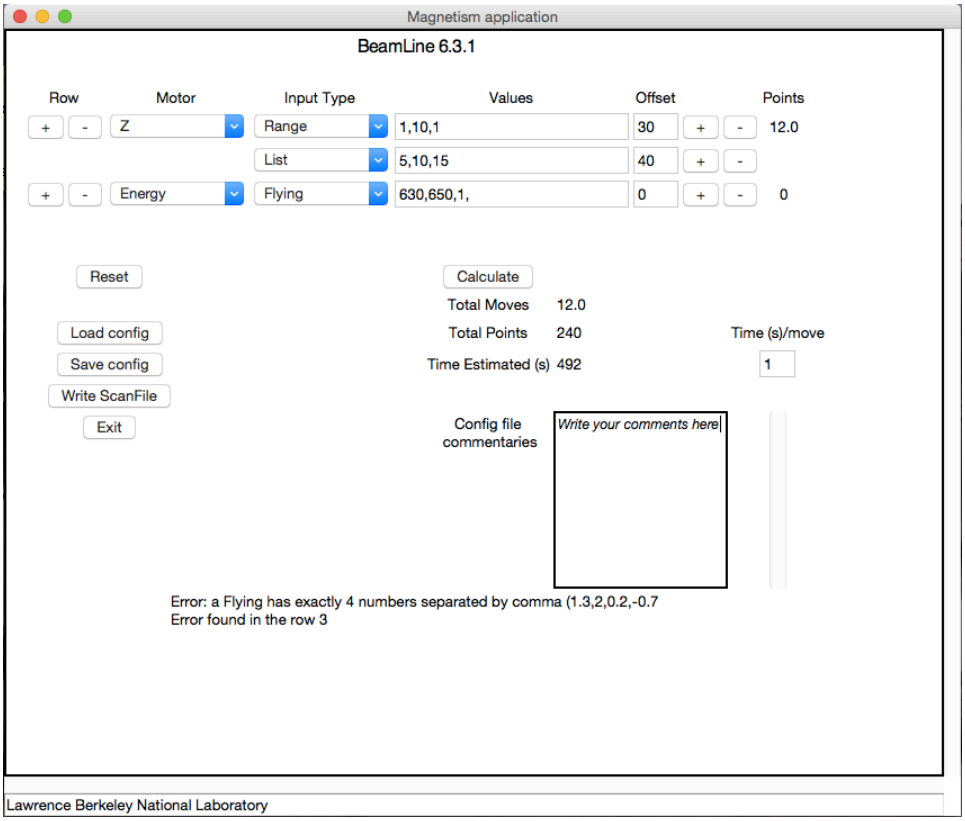

FIG. 3: Script manager graphical application

The application allows easily to insert and to delete motor row's according to the desired scan order. Also to add more input types and values under a specific motor.

The 'Offset' input box aids the user to define a starting value, which will be added to the first two numbers inserted in the value box. It is useful because it allows to run the same scan settings for the same sample regardless the sample holder or the separation between the samples.

The ‘Time(s)/move’ sets the initial time desired per move, which will be added to the fourth number of the input type Flying, if it makes part of the setting.

The ‘Calculate’ button tells the user different information for the inserted settings: total moves or number of lines of the script, total points that is proportional to the total time, and the estimated time for the run.

The ‘Reset’ button brings the GUI to its initial format.

The ‘Save config’ button creates a .ini file with the date of the application version, date of .ini file creation, the settings inserted and the commentaries inputted in the interface.

The ‘Load config’ button imports a previously saved configuration.

The ‘Write ScanFile’ button creates a .txt file with the inputted settings in a defined structure, readable by the Beamline software.

The algorithm contains an error handling in case the user inputs: the wrong type of data, or the incorrect number of values for a certain input type. It stops the action and generates a message describing the error. As Fig 12 shows.

4. CONCLUSION

There is Mn above the Ruthenium wedge layer observing a constant Mn X-ray absorption intensity in Fig 4 despite the Ru thickness. The Mn is oxidized identifying oxygen by the split peaks on L-edges and also comparing its signal with an actual oxidized Mn in Fig 5.

The TEY and luminescence techniques are complementary. The luminescence allows to measure the absorption around a hundred nanometers deeper into the sample but the TEY gives a less noise signal on the first few nanometers of the sample.

Comparing the Stoner-Wolfarth (SW) simulation results and the MH experimental data, one can conclude that the CoFe and NiFe layers follow the SW model but has smoother transitions on magnetization reversal, probably due to finite domain sizes.

The CoFe and NiFe layers present a biquadratic coupling exchange when the thickness of the Ruthenium wedge is $d_{ru} < 2.20$nm and $d_{ru} = 3.07$nm, as Fig 10 shows. The smaller the Ru wedge is the greater biquadratic coupling exchange is presented, finding a negative correlation.

The script manager is a helpful application for the users of the Beamline 6.3.1. Setting up big scans has been immensely simplified. Additionally, the software application is easy to use, to modify and to adapt to the new user needs. It also provides a better overview of the scan file created displaying the number of moves, the number of points, and the time estimated for the scan.

5. ACKNOWLEDGEMENT

I would like to thank Drs. Alpha T. N'Diaye and Elke Arenholz for mentoring me on this project, especially for their guidance and support throughout the internship, and also Dr. Jan Schmalhorst for providing the samples used in the experiments. I would like to thank Laleh Coté, as the undergraduate internship coordinator and the Office of Workforce Development that assured the excellence of the program. This work was supported in part by the U.S. Department of Energy, Office of Science, and Office of Workforce Development for Teachers and Scientists (WDTS) under the Science Undergraduate Laboratory Internship (SULI) program. The Advanced Light Source is supported by the

Director, Office of Science, Office of Basic Energy Sciences, of the U.S. Department of Energy under Contract No. DE-AC02-05CH11231.

6. REFERENCES

[1.] C Tannous and J Gieraltowski. "The Stoner–Wohlfarth model of ferromagnetism". European journal of physics. 29 (2008) 475–487

[2.] Stöhr, Joachim, Siegmann, Hans Christoph. *Magnetism From Fundamentals to Nanoscale Dynamics,* Springer Series in Solid-State Sciences (2006), pp 431-451

[3.] US Department of the Interior, US Geological Survey, *Mineral commodity summaries 2014,* USGS science for a changing world (2014), pp 128-129

[4.] Nachimuthu, P., Underwood, J. H., Kemp, C. D., Gullikson, E. M., Lindle, D. W., Shuh, D. K., Perera, "Performance Characteristics of Beamline 6.3.1 from 200 eV to 2000 eV at the Advanced Light Source", Proceedings of the Eighth International Conference on Synchrotron Radiation Instrumentation, 705 454 457 (2004)

[5.] Alexey I. Nesvizhskii. *Theory and Interpretation of L-shell X-ray Absorption Spectra*. University of Washington (2001)

[6.] C.T. Chen, Y. U. Idzerda, H.-J. Lin, N. V. Smith, G. Meigs, E. Chaban, G. H. Ho, F. Sette, "Experimental confirmation of the X-Ray Magnetic Circular Dichroism Sum Rules for Iron and Cobalt", Physical Review Letters, Volume 75, Number 1 (1995)

[7.] Python 2.7.8. July 2010. Python Software Foundation. US

[8.] PyCharm 4.0.4 January 2015. JetBrains s.r.o. Czech Republic

[9.] Anaconda 2.1.9 October 2013. Continuum Analytics. US

[10.] M. M. Grush, J. Chen, T. L. Stemmler, S. J. George, C. Y. Ralston, R. T. Stibrany, A. Gelasco, G. Christou, S. M. Gorun, J. E. Penner-Hahn, and S. P. Cramer, "Manganese L-Edge X-ray Absorption Spectroscopy of Manganese Catalase from

Lactobacillus plantarum and Mixed Valence Manganese Complexes", J. Am. Chem. Soc., 118, 65-69 (1996)

7. FIGURES

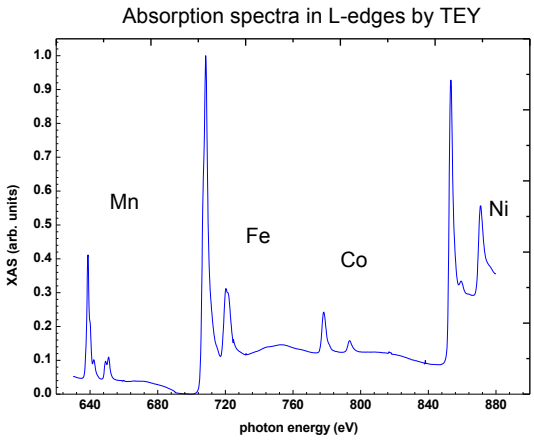

(a) XAS by TEY where d_{ru} = 0.31nm

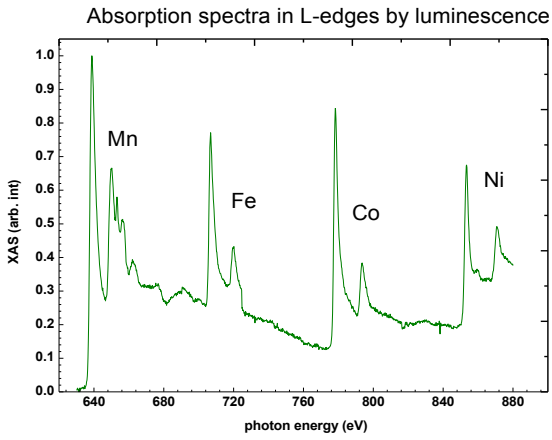

(b) XAS by luminescence where d_{ru} = 0.31nm

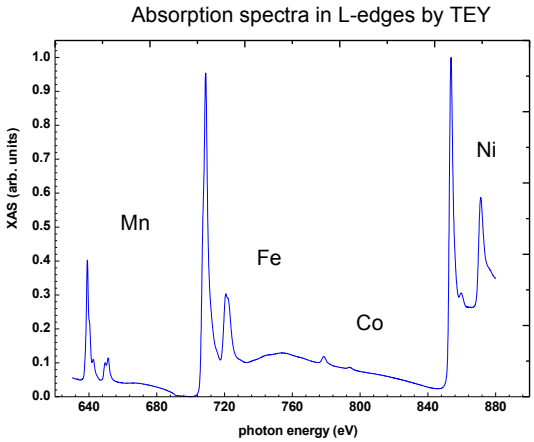

(c) XAS by TEY where d_{ru} = 3.07nm

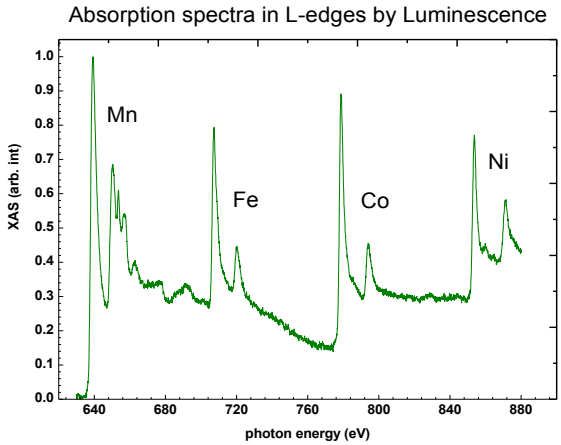

(d) XAS by luminescence where d_{ru} = 3.07nm

FIG. 4: XAS by TEY and luminescence where (a)(b) d_{ru} = 0.31nm and (c)(d) 3.07nm. Absorption intensity comparison between the two techniques when the Ruthenium wedge grows

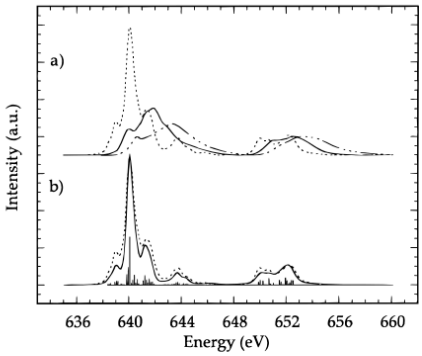

FIG. 5: Oxidation state shifts of manganese L-edge spectra: (a) Mn- (II)SO4 (dotted line), NBu4[Mn(III)4O2(O2CMe)7(pic)2] (solid line), and Mn(IV)O2 (dotted and dashed line); (b) Mn(II)SO4 (dotted line) and theoretical simulation (solid line). Image credit: Grush et al, 1996 [10]

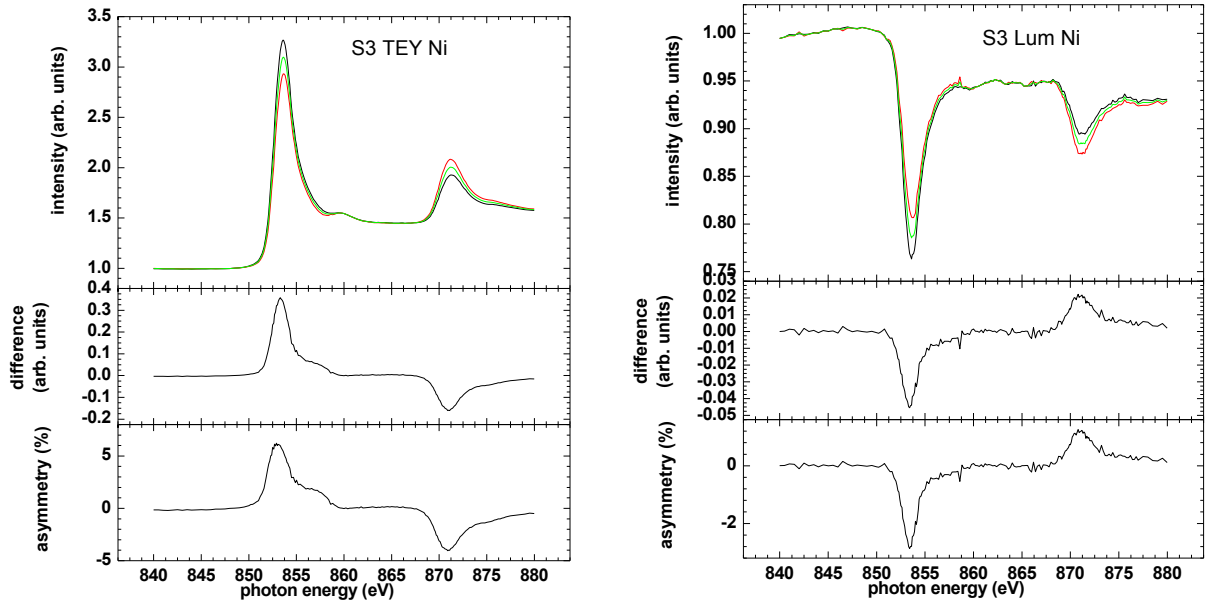

(a) XMCD by TEY of Ni where d_{ru}= 0.31nm

(b) XMCD by luminescence of Ni where d_{ru}= 0.31nm

FIG. 6: XMCD by (a) TEY and (b) luminescence where d_{ru}= 0.31nm. L-edges identification, difference and asymmetry analysis.

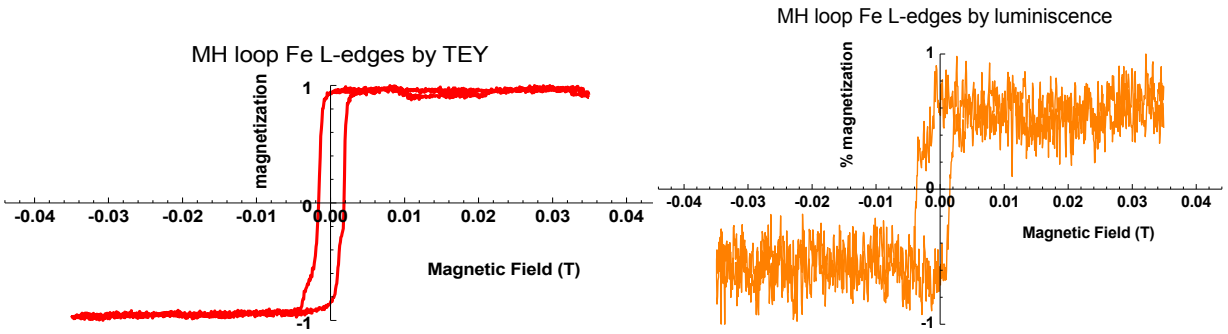

(a) MH by TEY of Fe where d_{ru}= 1.86nm

(b) MH by luminescence of Fe where d_{ru}= 1.86nm

FIG. 7: MH loop by (a) TEY and (b) luminescence where d_{ru}= 1.86nm

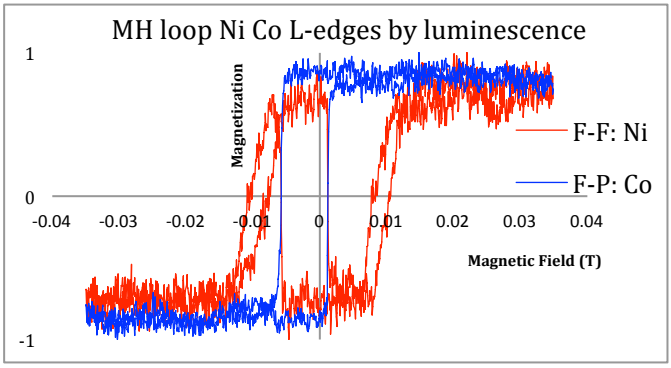

(a) MH luminescence where d_{ru}= 1.86nm

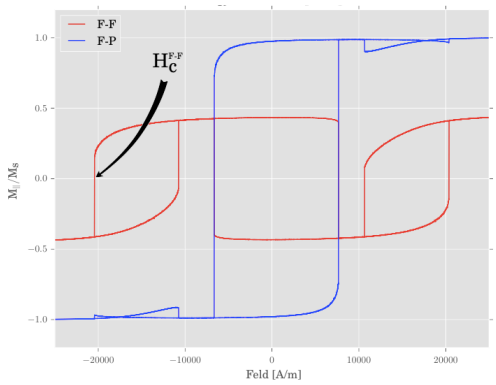

(b) SW model simulation. Antiferromagnetic layer coupling. Bilinear-coupling: $K_{21} = -14.0 \times 10-5$ J/m2

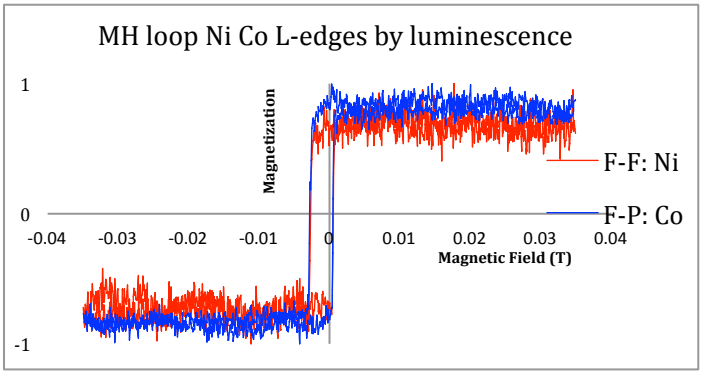

(c) MH luminescence where d_{ru}= 2.79nm

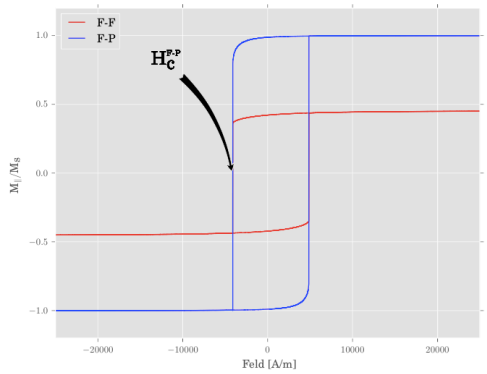

(d) SW model simulation. Ferromagnetic layer coupling. Bilinear-coupling: $K_{21} = 2.0 \times 10-5$ J/m2

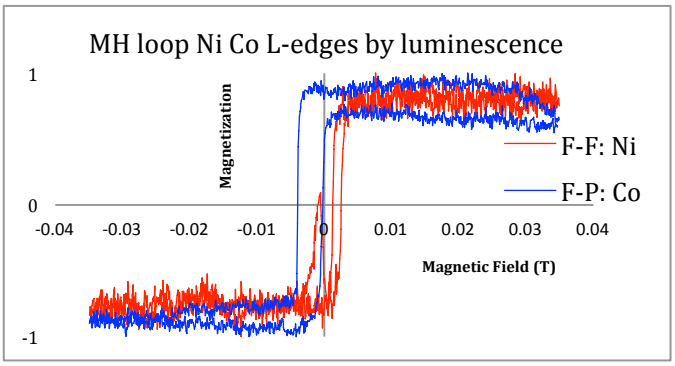

(e) MH luminescence where d_{ru}= 3.07nm

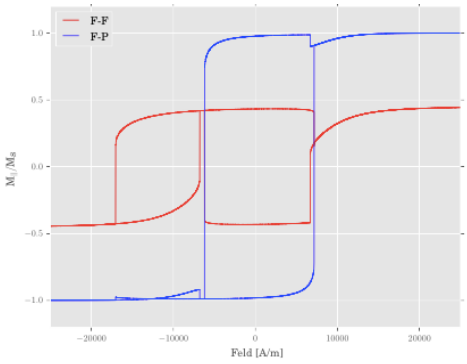

(f) SW model simulation. Antiferromagnetic layer coupling. Bilinear-coupling: $K_{21} = -10.5 \times 10-5$ J/m2

FIG. 8: comparison between (a)(c)(e) MH loops obtained experimentally and (b)(d)(f) SW model simulation done by the group of Jan Schmalhorst in Germany. Image (b)(d)(f) credit: Schmalhorst et al, 2013

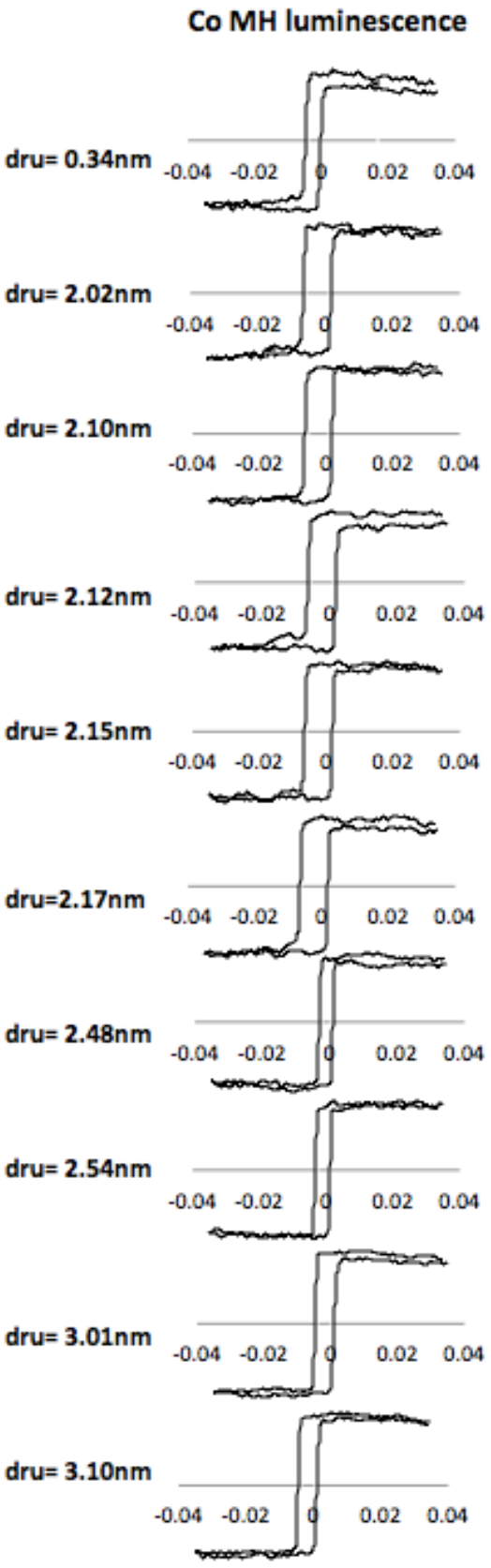

FIG. 9: Co MH luminescence evolution within d_{ru} from 0.34nm to 3.10nm

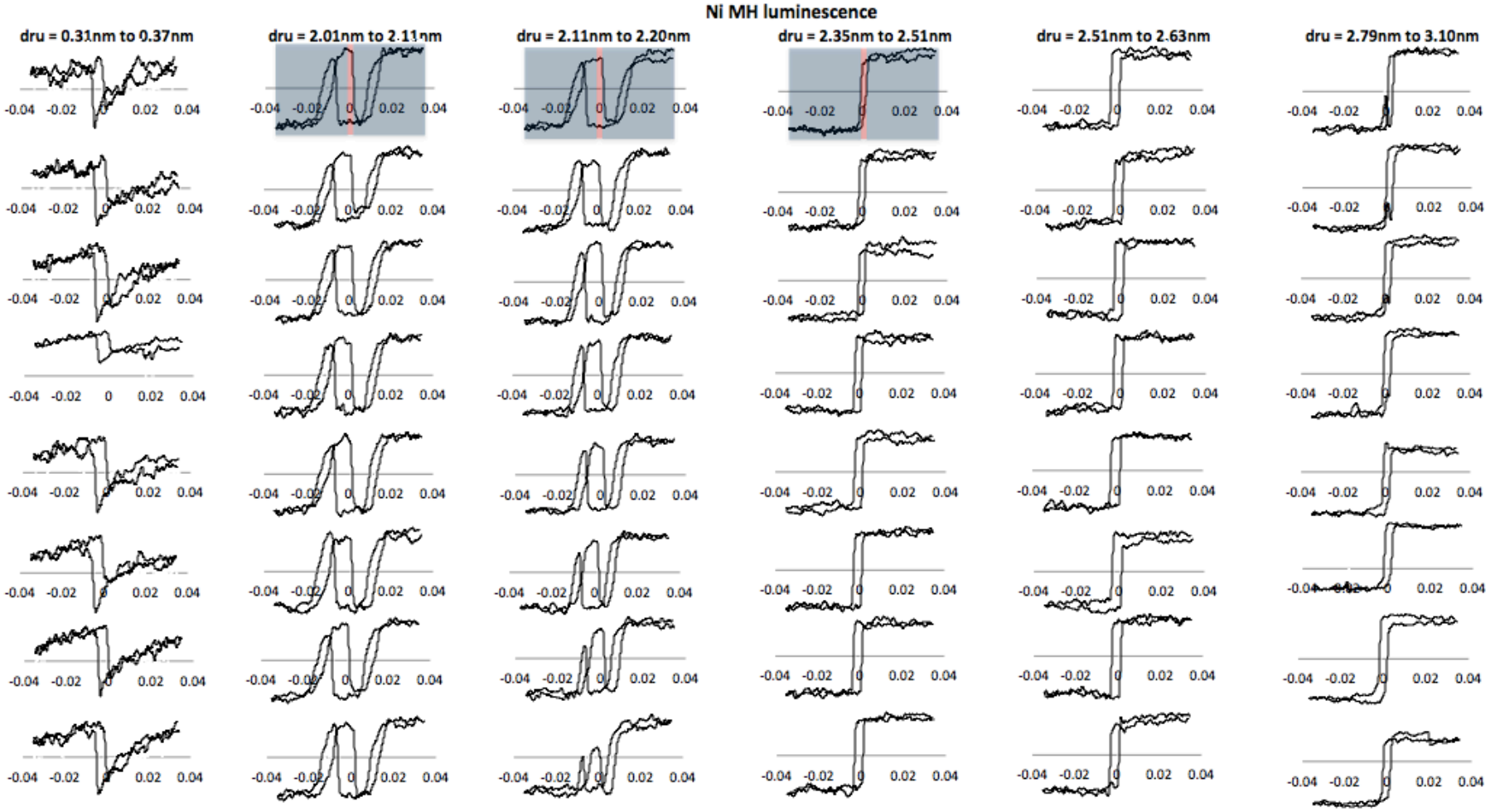

FIG. 10: Ni MH luminescence evolution within d_{ru} from 0.31nm to 3.10nm

```
__author__ = 'Juan Felipe Builes' + 'Alpha T. NDiaye'

import ...

class main():...

# Graphical static widgets
class gui(Frame):...

# Dynamic algorithm to display/modify the buttons, input boxes, entry boxes and labels
class displayBoxesMenusButtons():...

# Buttons actions
class script():


    def __init__(self, displayobject, objectGraphic):...

    # main function that summons the other functions
    # creates the text file
    def writeScanFile(self):...

    # Compiles a dictionary of the inputted motors
    def createDictionaries(self):...

    # Reads the inputted data in the GUI
    def readGui(self, j):...

    # Alpha's conditional loop to integrate the dictionaries into a variable
    # Variable that will be printed in a txt file in the 'writeScanFile' function
    def printMesh(self, meshField, i=0, line=''):...

    def saveConfig(self):...

    def loadConfig(self):...

    def resetConfig(self):...

    # Displays the info of the scan: moves, points and times
    def calculate(self):...

    def quitApp(self):...


if __name__ == '__main__':

    # creates a blank GUI
    root = Tk()
```

FIG. 11: software application class and functions' documentation

```
    elif self.display.inputType[j].get() == "Range":
            try:
                # Loop that adds the Off set to the values
                for k in range(0,2):
                    c[k] = float(c[k]) + float(self.display.inputBoxOffSet[j].get())
                # Calculate the points and the moves per motor
                self.pointsPerMotor = self.pointsPerMotor + math.ceil((float(c[1])-float(c[0]))/float(c[2]))
                self.movesPerMotor = self.movesPerMotor + math.ceil((float(c[1])-float(c[0]))/float(c[2]))
                e = np.arange(float(c[0]), float(c[1]), float(c[2]))
                # Add to the list 'l' that would be added to the dictionary
                for m in range(0, len(e)):
                    self.l.append(e[m])
            except:
                self.graphic.labelError = Label(self.graphic.frameThree, text="Error: a Range has exactly 3 "
                "numbers separated by comma: (start, stop, step) \nError found in the row " + str(j+1), justify =LEFT)
                self.graphic.labelError.grid(row=12, columnspan=18)
                self.error = True

    elif self.display.inputType[j].get() == "Flying":
            try:
                # Loop that adds the Off set to the values
                for k in range(0,2):
                    c[k] = float(c[k]) + float(self.display.inputBoxOffSet[j].get())
                # Add to the list 'l' that would be added to the dictionary
                self.l.append("flying({0}, {1}, {2}, {3})".format(float(c[0]), float(c[1]), float(c[2]), float(c[3])))
                # Calculate the points, the moves and the time per motor
                self.pointsPerMotor = self.pointsPerMotor + abs(math.ceil((float(c[1])-float(c[0]))/float(c[2])))
                self.movesPerMotor = self.movesPerMotor + 1
                self.time = math.ceil((float(c[1])-float(c[0]))/float(c[3]) + float(self.graphic.entryTime.get()))

            except:
                self.graphic.labelError = Label(self.graphic.frameThree, text="Error: a Flying has exactly 4 numbers "
                "separated by comma (1.3,2,0.2,-0.7 \nError found in the row " + str(j+1), justify =LEFT)
                self.graphic.labelError.grid(row=12, columnspan=18)
                self.error = True
    else:
        self.graphic.labelError= Label(self.graphic.frameThree, text="Error: the input type " + self.display.inputType[j].get() +
        " is unknown \nError found in the row " + str(j+1), justify =LEFT)
        self.graphic.labelError.grid(row=12, columnspan=18)
        self.error = True
else:
    self.graphic.labelError = Label(self.graphic.frameThree, text="Error: you must select an input type \nError "
    "found in the row " + str(j+1), justify =LEFT)
    self.graphic.labelError.grid(row=12, columnspan=18)
    self.error = True
```

FIG. 12: software application error handling